Hindawi
Mathematical Problems in Engineering
Volume 2022, Article ID 5344759, 12 pages
https://doi.org/10.1155/2022/5344759

Research Article

Dynamics of Unsteady Flow of Chemically Reactive Upper-Convected Maxwell Fluid with Temperature-Dependent Viscosity: Keller Box Analysis

Zia Ullah,[1] Samina Yasmin,[1] Jihad Younis,[2] Ameer Abdullah,[1] Shahid Abbas,[1] and Asif Shah[1]

[1]*Department of Mathemtics, University of Lahore, Sargodha Campus, Sargodha, Pakistan*
[2]*Aden University, Khormaksar, P. O. Box 6014, Aden, Yemen*

Correspondence should be addressed to Jihad Younis; jihadalsaqqaf@gmail.com

Received 1 November 2021; Revised 5 January 2022; Accepted 18 February 2022; Published 17 June 2022

Academic Editor: Salman Saleem

The heat and mass transfer characteristics of unsteady flow of incompressible chemically reactive upper-convected Maxwell fluid along a stretching surface in the presence of temperature-dependent viscosity has been studied. The theoretical analysis on heat and mass transfer over a stretching sheet is investigated for numerical analysis. With the use of stream function formulation, the governing boundary layer equations of momentum, energy, and concentration are reduced to a set of linked ordinary differential equations. The nonlinear ordinary differential equations are then solved numerically by using the Keller Box method. The physical behavior of governing parameters on velocity, temperature, and concentration profiles and the local skin friction coefficient and heat and mass transfer rates are graphed and tabulated. The physical impact of Maxwell parameter β, unsteadiness parameter M, Schmidt number Sc, Prandtl number Pr, reaction rate parameter γ, and variable viscosity parameter ε on the heat and mass transfer has been examined along the stretching surface numerically. The novelty of the present work is to examine the importance of destructive reaction and contractive reaction on the dynamics of upper-convected Maxwell fluid flow in the presence of temperature-dependent viscosity effects. It is observed an interesting behavior of temperature distribution and concentration profile is noted for lower value of viscosity parameter ε in the presence of chemical reaction. It is also found that skin friction and the rate of heat transfer are decreased by increasing the variable viscosity parameter ε.

1. Introduction

Heat and mass transfer together with the momentum of laminar boundary flow on a stretching sheet is important both theoretically and practically due to its wide application in polymer technology. The flow characteristics of non-Newtonian fluids are quite different in comparison to Newtonian fluids. In order to obtain a clear idea of non-Newtonian fluids and their various applications, it is necessary to study their flow behavior. Heat is a sort of energy that is transferred between different temperature systems or objects. The mass transfer phenomenon is used in various scientific disciplines for different systems and mechanisms that involve molecular and convective transport of atoms and molecules. The dynamics of a material having the properties of elasticity and viscosity when undergoing deformation is a fundamental topic in fluid dynamics. This kind of material referred to as Maxwell fluid has attracted the attention of many researchers due to its wide industrial and technical applications. The upper-convected Maxwell model can be described as the generalization of the Maxwell material for the case of large deformation using the upper-convected time derivative in the coordinate system stretching with the fluid. The study of boundary layer flow over a stretching surface is always essential from a technological point due to its multiple applications in engineering for non-Newtonian fluid flow mechanisms such as printer's ink, melts, slurries, and groceries. Siddheshwar

et al. [1] worked on forced flow mechanism for Newtonian liquids along the various stretchable geometries numerically. Aman et al. [2] developed a fractional mathematical model of Maxwell fluid along the porous geometry with second-order slip effects numerically. A similarity analysis was presented by Abd El-Aziz [3] to investigate a special distribution of the stretching velocity and surface heat flux for unsteady boundary layers over a stretched sheet. Abel et al. [4] performed a nonisothermal analysis on the stretching shape with heat flux and variable viscosity effects numerically.

In all of the mentioned studies, fluid viscosity has been assumed to be a constant function of temperature within the boundary layer. However, it is known that the physical properties of the fluid may change significantly when exposed to internal generated temperature. Viscosity depends strongly on temperature. In liquids, it usually decreases with increasing temperature, whereas in gases, viscosity increases with increasing temperature. Hassanein [5] developed a mathematical analysis for continuous shapes to examine heat transfer with variable viscosity. Khan et al. [6] analyzed the viscosity change in the Maxwell fluid mechanism under the influence of solutal stratification effects. Khan et al. [7] discussed the technical note for thin film flow behavior over shrinking geometry with thermal properties. Mukhopadhyay and Bhattacharyya [8] discussed the effects of chemical reactions on unsteady mixed convection flow and heat transfer over a porous stretching sheet. Some authors [9, 10] studied the effects of ohmic dissipation on viscoelastic flow and heat transfer under different conditions. Cortell [11] examined the numerical phenomena on second-grade viscoelastic flow to predict the mass and momentum transfer behavior across the porous mechanism theoretically. He obtained valid solutions compared to the previous mentioned results. An analytical solution of chemically reacting species in viscous flow across the plane elastic geometry under homogeneous reactions has been illustrated by Andersson et al. [12]. The technical problem about thermocapillary over a stretchable shape for thin film flow has been studied in [13, 14].

Elbashbeshy and Bazid [15] examined the velocity behavior of flow for unsteadiness along the stretching geometry numerically. Tsai et al. [16] studied the quiescent fluid medium problem with heat source effects across the unsteady stretching shape. The flow behavior of Maxwell fluid in a channel has been obtained theoretically in [17]. Chamkha et al. [18] produced similar results in porous shape for mass and heat behavior with chemical reaction. The mass transfer characteristics along the stretching geometry under slip and suction/injection effects by using shooting technique have been obtained by Bhattacharyya et al. [19, 20]. Gupta and Gupta [21] illustrated the mass transfer phenomena with blowing or suction impacts along the stretching surface mathematically. Ishak et al. [22] investigated the heat mechanism on permeable geometry with stretching and wall temperature effects numerically. The combined effects of transpiration and suction/blowing on unsteady mixed convection flow via a stretching sheet were studied by Mukhopadhyay and Vajravelu [23].

The flow of fluids may be categorized into Newtonian fluid flow, viscoelastic fluid flow, a flow of non-Newtonian fluid with time-dependent viscosity, and the flow of non-Newtonian fluids with time-independent viscosity. However, there exists no fluid flow which accurately fits the definition of a Newtonian fluid flow (i.e., shear stress is proportional to the rate of deformation). By taking an idea from Mukhopadhyay and Bhattacharyya [8], the unsteady two-dimensional flow of Maxwell fluid in the presence of variable viscosity and chemical reaction has been studied. The governing partial differential equations are transformed into ordinary ones using appropriate transformations, and the reduced ordinary differential equations are solved numerically using the Keller Box scheme. With the use of graphical representations, the impacts of controlling factors on velocity, temperature, and concentration fields with their slopes are explored and analyzed.

2. Research Methodology

Over an unstable stretched sheet, we study laminar boundary-layer two-dimensional flow and mass transfer of an incompressible non-Newtonian Maxwell fluid. Let C_w represent the concentration on the sheet surface and C_∞ represent the concentration away from the sheet. Furthermore, the species' reaction is a first-order homogeneous chemical reaction with a rate k_1 that varies with time. We assume that the fluid and mass fluxes are constant at time $t < 0$. At $t = 0$, the unsteady fluid and mass fluxes begin. The sheet emerges from a slit at the origin $(x, y = 0)$ and moves with a nonuniform velocity $U(x,t) = bx/1 - \alpha t$, where b and α are positive constants with dimensions (time)-1, b is the initial stretching rate, and $b/1 - \alpha t$ is the effective stretching rate that increases with time. The material properties of the extruded sheet may change over time in the case of polymer extrusion. The governing equations are given as follows [8]:

In Figure 1, u and v are the components of velocity in x and y directions, μ and ν are the fluid's dynamic and kinematic viscosity, C is the fluid's concentration (of the species), and D is the diffusing species' diffusion coefficient. Furthermore, $k_1(t) = k_0/1 - \alpha t$ is the time-dependent reaction rate, where $k1 > 0$ denotes destructive reaction and $k_1 < 0$ denotes constructive reaction, κ_0 is a constant, $\lambda = \lambda_0(1 - \alpha t)$ is the period's relaxation time, λ_0 is a constant, T denotes temperature, and T_∞ denotes free-stream temperature.

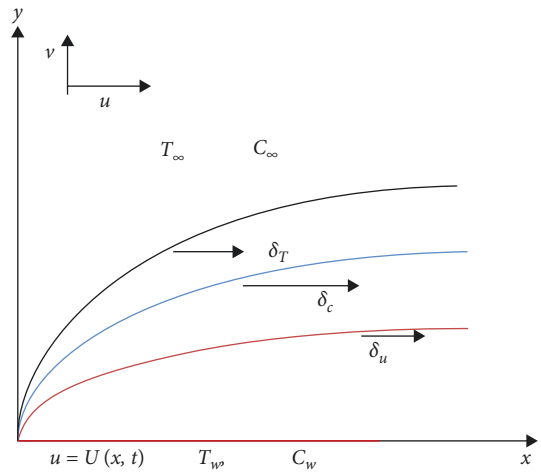

Figure 1: Coordinate system and flow geometry.

$$\frac{\partial u}{\partial x} + \frac{\partial v}{\partial y} = 0, \tag{1}$$

$$\frac{\partial u}{\partial t} + u\frac{\partial u}{\partial x} + v\frac{\partial u}{\partial y} + \lambda\left(u^2\frac{\partial^2 u}{\partial x^2} + v^2\frac{\partial^2 u}{\partial y^2} + 2uv\frac{\partial^2 u}{\partial x \partial y}\right) = \frac{1}{\rho}\frac{\partial}{\partial y}\left(\mu\frac{\partial u}{\partial y}\right), \tag{2}$$

$$\frac{\partial T}{\partial t} + u\frac{\partial T}{\partial x} + v\frac{\partial T}{\partial y} = \frac{\kappa}{\rho c_p}\frac{\partial^2 T}{\partial y^2}, \tag{3}$$

$$\frac{\partial C}{\partial t} + u\frac{\partial C}{\partial x} + v\frac{\partial C}{\partial y} = D\frac{\partial^2 C}{\partial y^2} - k_1(C - C_\infty). \tag{4}$$

The suitable boundary conditions for the problem are given as follows:

$$\begin{aligned} &u = U(x,t); v = 0; C = C_w(x,t); T = T_w \text{ at } y = 0, \\ &u \longrightarrow 0, C \longrightarrow C_\infty, T \longrightarrow T_\infty \text{ as } y \longrightarrow \infty. \end{aligned} \tag{5}$$

Here, C_w is concentration at the sheet surface equal to $C_w(x,t) = C_\infty + bx(1-\alpha t)^{-2}$, where C_∞ is the concentration far away from the surface, $T_w = T_\infty + T_0/x$ is variable temperature, T_0 is constant, κ is the thermal conductivity of fluid, and c_p is the specific heat.

2.1. Stream Function Formulation. The following physical dimensionless similarity transformations along with the stream function formulation were used by Mukhopadhyay [8, 23] to reduce the governing partial differential equations into the system of ordinary differential equations:

$$u = \frac{\partial \psi}{\partial y}, v = -\frac{\partial \psi}{\partial y}, \phi = \frac{C - C_\infty}{C_w - C_\infty}, \theta = \frac{T - T_\infty}{T_w - T_\infty}, \tag{6}$$

where ψ is the stream function and η is the similarity variable.

$$\begin{aligned} \eta &= \sqrt{\frac{c}{(1-\alpha t)\nu}}y, \\ \psi &= \sqrt{\frac{\nu c}{(1-\alpha t)}}x f(\eta), \\ C &= C_\infty + bx(1-\alpha t)^{-2}\phi(\eta), \\ T &= T_\infty + \frac{T_0}{x}\theta(\eta), \\ \mu &= \mu_\infty[1 + \gamma(T - T_\infty)]. \end{aligned} \tag{7}$$

With the help of the above relations, the governing partial differential equations are finally reduced to nonlinear ordinary differential equations given as follows:

$$M\left(\frac{\eta}{2}f'' + f'\right) + (f')^2 - ff' + \beta\left(f^2 f''''' - 2f''' f' f\right) = f''''' (1 + \varepsilon\theta) + f''\varepsilon\theta, \tag{8}$$

$$\theta''' + \Pr\left(f\theta' + \theta f'\right) = 0, \tag{9}$$

$$M\left(\frac{\eta}{2}\phi' + 2\phi\right) + f'\phi - \phi' f = \frac{1}{Sc}\phi'' - \gamma\phi, \tag{10}$$

where $\Pr = \mu c_p/\kappa$ is the Prandtl number, η is the similarity variable, θ is the dimensionless temperature, $\nu = \mu/\rho$ is the kinematic fluid viscosity, $\varepsilon = \gamma(T_w - T_\infty)$ is the variable viscosity parameter, $Sc = \nu/D$ is the Schmidt number, $M = \alpha/b$is the unsteadiness parameter, $\beta = b/\lambda_0$ is the Maxwell parameter, and $\gamma = k0/b$is the reaction rate parameter. Moreover, $\gamma > 0$ shows the destructive reaction and $\gamma < 0$ shows reaction is constructive, but $\gamma = 0$ corresponds to no reaction.

The boundary conditions in (5) then becomes

$$\begin{aligned} &f' = 1, f = 0, \theta = 1, \phi = 1 \text{ at } \eta = 0, \\ &f' \longrightarrow 0, \theta \longrightarrow 0, \phi \longrightarrow 0 \text{ as } \eta \longrightarrow \infty. \end{aligned} \tag{11}$$

The mathematical expression for skin friction is $C_{fx} = \tau_w/\rho U_\infty^2$, the Nusselt number is $N_{u_x} = xq_w/\kappa(T_w - T_\infty)$, and the value of Schmidt number is $\mathrm{Sc} = \nu/D$ defined as the ratio of momentum diffusivity and mass diffusivity. It is used to characterize fluid flows in which there are simultaneous momentum and mass diffusion convection process. The mathematical expression for the Sherwood number is $Sh_x = x\phi_m/D(C_w - C_\infty)$. The values of τ_w, q_w, and ϕ_m are $\tau_w = \mu(\partial u/\partial y)_{y=0}, q_w = -\kappa(\partial T/\partial y)_{y=0}$, and $\phi_m = -D(\partial C/\partial y)_{y=0}$.

Thus, the values of skin friction, Nusselt number, and Sherwood number are given by $R_{e_x}^{1/2} C_{f_x} = f''(0), R_{e_x}^{-1/2} N_{u_x} = -\theta'(0)$, and $R_{e_x}^{-1/2} Sh_x = -\phi'(0)$.

2.2. Computational Technique. The coupled partial differential equations for the above model are reduced into a set of ordinary differential equations with the help of suitable stream function formulation. The reduced nonlinear ordinary differential equations (8)–(10) along with the boundary conditions in (11) are solved numerically by using the Keller Box scheme with an iterative method. We start by introducing new independent variables $p(\eta), q(\eta), t(\eta)$, and $v(\eta)$ by using the following equation:

$$\begin{aligned} &f' = p, p\imath = q, \phi' = v, \theta' = t, \\ &\tau_w = \mu\left(\frac{\partial u}{\partial y}\right)_{y=0}, q_w = -\kappa\left(\frac{\partial T}{\partial y}\right)_{y=0}, \phi_m = -D\left(\frac{\partial C}{\partial y}\right)_{y=0}. \end{aligned} \tag{12}$$

$R_{e_x}^{1/2} C_{f_x} = f''(0), R_{e_x}^{-1/2} N_{u_x} = -\theta'(0), R_{e_x}^{-1/2} Sh_x = -\phi'(0).$

To overcome the difficulty of solving the equations, equations (8)–(11) become

$$(1 + \varepsilon\theta)q' + \varepsilon qt - M\left(\frac{\eta}{2}q + p\right) - p^2 + fq - \beta\left(f^2 q' - 2fpq\right) = 0, \tag{13}$$

$$t' + \Pr(ft + \theta p) = 0, \tag{14}$$

$$\frac{1}{Sc}v' - \gamma\phi - M\left(\frac{\eta}{2}v + 2\phi\right)p\phi + vf = 0. \tag{15}$$

The reduced boundary conditions are as follows:

$$\begin{aligned} &f = 0, p = 1, \theta = 1, \phi = 1 \text{ at } \eta = 0, \\ &p \longrightarrow 0, \theta \longrightarrow 0, \phi \longrightarrow 0 \text{ as } \eta \longrightarrow \infty. \end{aligned} \tag{16}$$

We now consider the segment η_{n-1} and η_n with $\eta_{n-1/2}$ as the midpoint given as follows:

$$\eta_0 = 0, \eta_n = \eta_{n-1} + h_n, \eta_n = \eta_\infty. \tag{17}$$

The central difference form and average form are given as follows:

$$f' = \frac{f_n - f_{n-1}}{h}, f = \frac{f_n + f_{n-1}}{2} = f_{n-1/2}, \tag{18}$$

$$f_n - f_{n-1} - \frac{1}{2}h_n(p_n + p_{n-1}) = 0, \tag{19}$$

$$p_n - p_{n-1} - \frac{1}{2}h_n(q_n + q_{n-1}) = 0, \tag{20}$$

$$\theta_n - \theta_{n-1} - \frac{1}{2}h_n(t_n + t_{n-1}) = 0, \tag{21}$$

$$\phi_n - \phi_{n-1} - \frac{1}{2}h_n(v_n + v_{n-1}) = 0. \tag{22}$$

By applying equations (18)–(22), governing equations (13)–(16) become

$$\left[1+\frac{1}{2}\varepsilon(\theta_n+\theta_{n-1})\right](q_n-q_{n-1})+\frac{1}{4}h_n\varepsilon(t_n+t_{n-1})(q_n+q_{n-1})$$
$$-\frac{1}{2}Mh_n\left(\frac{\eta}{2}(q_n+q_{n-1})+(p_n+p_{n-1})\right)$$
$$-\frac{h_n}{2}(p_n+p_{n-1})^2+\frac{1}{4}h_n(f_n+f_{n-1})(q_n+q_{n-1})-\beta\frac{h_n}{4}\left[(f_n+f_{n-1})^2\frac{(q_n-q_{n-1})}{h_n}-(f_n+f_{n-1})(p_n+p_{n-1})(q_n-q_{n-1})\right]=0, \tag{23}$$

$$(t_n-t_{n-1})+\frac{h_n}{4}\Pr((\theta_n+\theta_{n-1})(p_n+p_{n-1})+(f_n+f_{n-1})(t_n+t_{n-1}))=0, \tag{24}$$

$$\frac{1}{Sc}(\nu_n-\nu_{n-1})-\gamma\frac{h_n}{2}(\phi_n+\phi_{n-1})-$$
$$M\frac{h_n}{2}\left[\frac{\eta}{2}(\nu_n+\nu_{n-1})+2(\phi_n+\phi_{n-1})\right]-\frac{h_n}{4}(p_n+p_{n-1})(\phi_n+\phi_{n-1}) \tag{25}$$
$$+\frac{h_n}{4}(f_n+f_{n-1})(\nu_n+\nu_{n-1})=0,$$

along with boundary conditions

$$f_0=0,p_0=1,\theta_0=1,\phi_0=1\text{ at }\eta=0,$$
$$p_0\longrightarrow 0,\theta_0\longrightarrow 0,\phi_0\longrightarrow 0\text{ as }\eta\longrightarrow\infty. \tag{26}$$

Now, by applying the iterative Newton–Raphson method for smooth algorithm, we get

$$f_n^{k+1}=f_n^k+\delta f_n^k,$$
$$q_n^{k+1}=q_n^k+\delta q_n^k,\theta_n^{k+1}=\theta_n^k+\delta\theta_n^k,$$
$$\phi_n^{k+1}=\phi_n^k+\delta\phi_n^k,t_n^{k+1}=t_n^k+\delta t_n^k, \tag{27}$$
$$\nu_n^{k+1}=\nu_n^k+\delta\nu_n^k,p_n^{k+1}=p_n^k+\delta p_n^k.$$

As in the standard Newton–Raphson technique, we neglect all appearances of powers of δ greater than the first power and hence equations become

$$\delta f_n-\delta f_{n-1}-\frac{1}{2}h_n(\delta p_n+\delta p_{n-1})=(r_1)_n, \tag{28}$$

$$\delta p_n-\delta p_{n-1}-\frac{1}{2}h_n(\delta q_n+\delta q_{n-1})=(r_2)_n, \tag{29}$$

$$\delta\theta_n-\delta\theta_{n-1}-\frac{1}{2}h_n(\delta t_n+\delta t_{n-1})=(r_3)_n, \tag{30}$$

$$\delta\phi_n-\delta\phi_{n-1}-\frac{1}{2}h_n(\delta\nu_n+\delta\nu_{n-1})=(r_4)_n. \tag{31}$$

Again, by using equations (27)–(31) in equations (23)–(26), the reduced form of equations is given as follows:

$$(a_1)_n\delta q_n+(a_2)_n\delta q_{n-1}+(a_3)_n\delta p_n+(a_4)_n\delta p_{n-1}+(a_5)_n\delta f_n+(a_6)_n\delta f_{n-1}=(r_5)_n,$$
$$(b_1)_n\delta t_n+(b_2)_n\delta t_{n-1}+(b_3)_n\delta\theta_n+(b_4)_n\delta\theta_{n-1}+(b_5)_n\delta p_n+(b_6)_n\delta p_{n-1}+(b_7)_n\delta f_n+(b_8)_n\delta f_{n-1}=(r_6)_n, \tag{32}$$
$$(c_1)_n\delta\nu_n+(c_2)_n\delta\nu_{n-1}+(c_3)_n\delta\phi_n+(c_4)_n\delta\phi_{n-1}+(c_5)_n\delta p_n+(c_6)_n\delta p_{n-1}+(c_7)_n\delta f_n+(c_8)_n\delta f_{n-1}=(r_7)_n.$$

We recall the boundary conditions that can be satisfied exactly with no iteration. Therefore, in order to keep up these correct values in all iterates, we take

$$\begin{aligned}
\delta f_0 &= 0,\\
\delta p_0 &= 1,\\
\delta \theta_0 &= 1,\\
\delta \phi_0 &= 1,\\
\delta p_n &= 0,\\
\delta \theta_n &= 0,\\
\delta \phi_n &= 0.
\end{aligned} \tag{33}$$

Now, this is a very important step to arrange the above difference equations in matrix form. If it is carried out incorrectly, then either the method becomes very inefficient due to the absence of any discernible structure in the matrix or the matrix solution method breaks down due to having a singular matrix (determinant = 0) or submatrix. The matrix form is given as

$$\begin{aligned}
A\delta &= r,\\
[A] &= \begin{bmatrix} [A_1][C_1][B_2][A_2][C_2] & \cdots & \cdots \\ \vdots & \ddots & \vdots \\ \vdots & \cdots & [B_{n-1}][A_{n-1}][C_{n-1}][B_n][A_n] \end{bmatrix},\\
[\delta] &= \begin{bmatrix} [\delta_1] \\ [\delta_2] \\ \vdots \\ [\delta_{n-1}] \\ [\delta_n] \end{bmatrix},\\
[r] &= \begin{bmatrix} [r_1] \\ [r_2] \\ \vdots \\ [r_{n-1}] \\ [r_n] \end{bmatrix}.
\end{aligned} \tag{34}$$

3. Analysis and Discussion of Results

The numerical computations of Maxwell fluid are executed for several values of dimensionless parameters involved in the equations such as variable viscosity parameter (ε), the Prandtl number (Pr), the Maxwell parameter (β), and the unsteadiness parameter M. To illustrate the computed results, some figures are plotted and physical explanations are given for velocity $f'(\eta)$, concentration $\phi(\eta)$, and temperature $\theta(\eta)$ with their slopes. Table 1 presents the validated numerical data for skin friction $f''(\eta)$ for accuracy of results by comparing them with existing results available in the study by Chamkha et al. [18] and Mukhopadhyay and Bhattacharyya [8]. The validated results with good agreement are found by keeping unsteady flow of incompressible Newtonian flow fluid $\beta = 0$ and $\varepsilon = 0 \cdot 1$. The most favorable numerical results are obtained by adding the energy equation to the present phenomena.

Figures 2(a)–2(c)) present the physical behavior of $f'(\eta), \theta(\eta)$, and $\phi(\eta)$ profiles for numerous values of $\varepsilon = 0 \cdot 1, 0 \cdot 5, 1 \cdot 0$, and $1 \cdot 5$ with some fixed parameters. From Figure 2(a), it is noted that the fluid velocity becomes maximum at a higher value of $\varepsilon = 1 \cdot 5$ while the minimum value of velocity profile is examined at a lower value of $\varepsilon = 0 \cdot 1$. In Figure 2(b), an interesting behavior of the temperature profile is reported for various values of ε with chemical reaction effects. The concentration profile increases with lower value of ε but decreases as ε increases with prominent variations in Figure 2(c) in the presence of chemical reaction. The maximum value of concentration is noted at lower ε. The temperature profile is increased with suitable variations at $\varepsilon = 0 \cdot 1$ but decreases as the parameter ε decreases significantly. In the presence of variable viscosity, the prominent behavior in concentration is illustrated for each value and temperature distribution is also found to be in good agreement.

Figures 3(a)–3(c) demonstrate fluid velocity profile, fluid temperature profile, and fluid concentration profile for the various values of Prandtl number $\mathrm{Pr} = 0 \cdot 1, 1 \cdot 0, 3 \cdot 0$, and $7 \cdot 0$ by keeping other parameters $\beta = 1 \cdot 4, S_c = 2 \cdot 5, \varepsilon = 3 \cdot 0, \gamma = 0 \cdot 4$, and $M = 0 \cdot 3$ constant along the stretchable surface. The velocity profile increases

Table 1: The values of $\mathbf{f}''(\eta)$ against unsteadiness parameter M with $\beta = 0$ and $\varepsilon = 0 \cdot 1$.

M	Chamkha et al. [18]	Mukhopadhyay and Bhattacharyya [8]	Present analysis
0.8	−1.261512	−1.261479	−1.200336
1.2	−1.378052	−1.377850	−1.311544

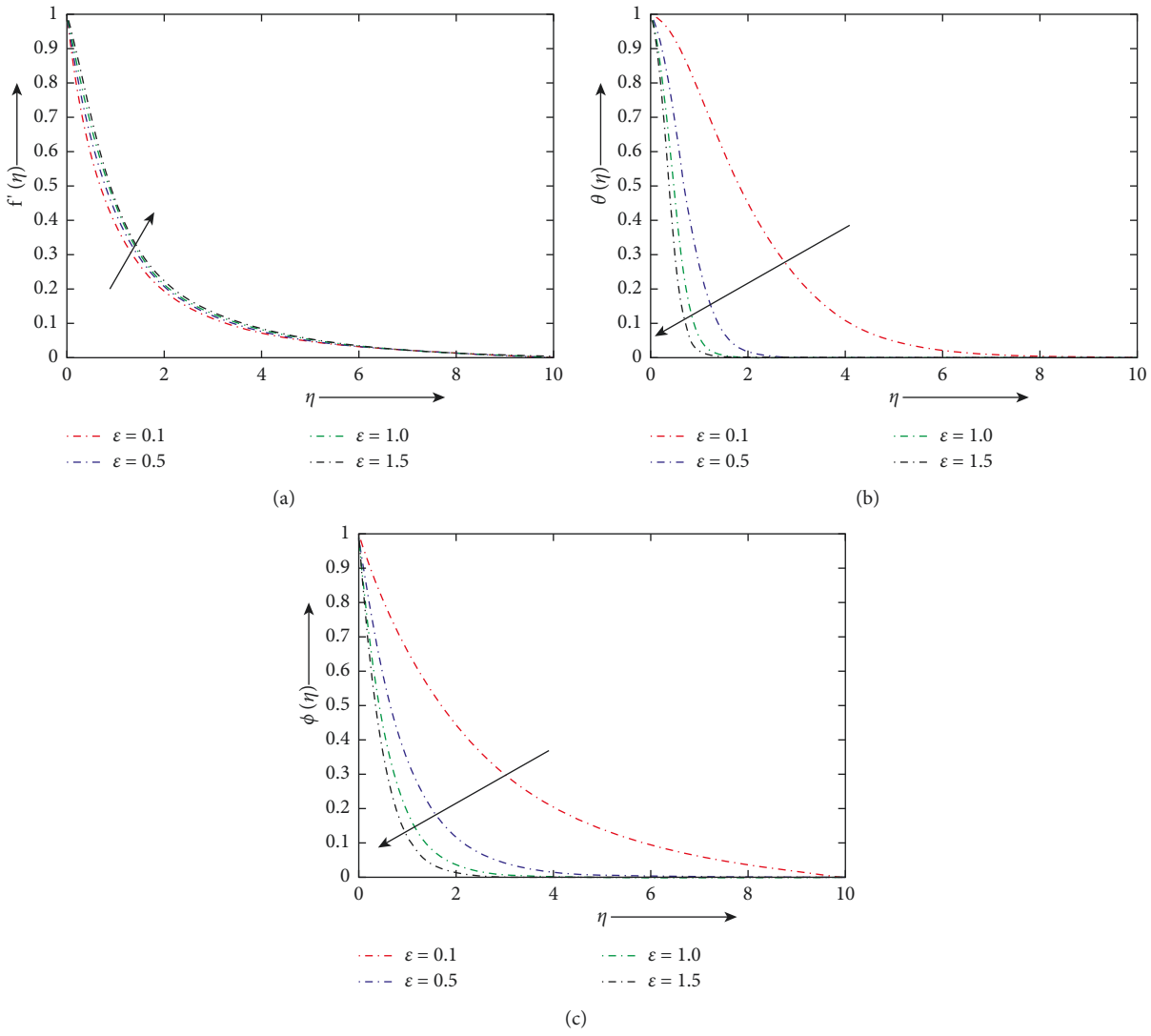

Figure 2: (a–c) Graphical representation of $\mathbf{f}'(\eta)$, $\theta(\eta)$, and $\phi(\eta)$ against temperature-dependent viscosity parameter ε with some fixed parameters.

with a lower value of Pr = 0 · 1 and gradually decreases with increasing Pr in Figure 3(a). The maximum increasing behavior in temperature is depicted at a lower value of Pr = 0 · 1, but this decreases as the value of Pr increases with prominent variations in Figure 3(b) significantly. The similar trend in concentration is examined for each value of Pr graphically, but the concentration increases with decreasing Pr values by satisfying the given boundary conditions in Figure 3(c). In the presence of viscosity effects, a suitable change is examined in velocity and temperature but a similar trend is examined in concentration for ε. The suitable response in concentration is illustrated in the presence of ε. The fluid flow caused solely, and the concentration is maximum than free-stream concentration along the stretching sheet.

From Figures 4(a)–4(c), it is concluded that the fluid velocity is maximum along the surface of a given shape for a lower value of $\beta = 0 \cdot 1$ and the minimum value is obtained at the largest value of $\beta = 2 \cdot 0$ with good response. The velocity profile showed good variations in the presence of $\varepsilon = 2 \cdot 5$ in Figure 4(a). In Figure 4(b), the temperature profile is represented graphically for different values of $\beta = 0 \cdot 1, 0 \cdot 5, 1 \cdot 0$, and $2 \cdot 0$ by keeping other parameters constant. In Figure 4(c), it is noted that the concentration

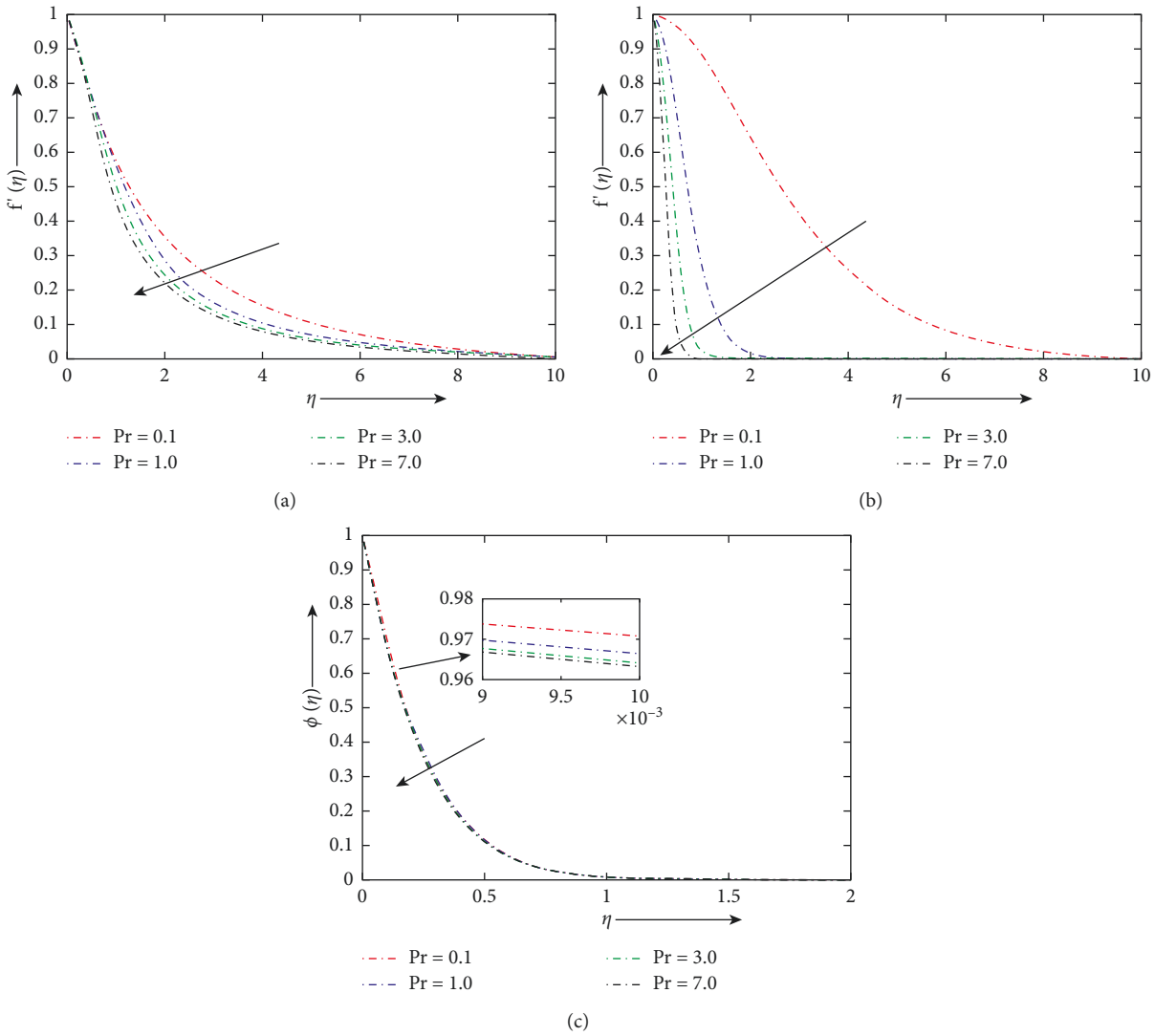

Figure 3: (a–c) Graphical representation of $\mathbf{f}'(\eta)$, $\theta(\eta)$, and $\phi(\eta)$ against Prandtl number Pr with some fixed parameters.

distribution has a similar behavior at lower values of β but increasing change is noted as β increases. It is observed that temperature θ shows similar behavior for each value of β and gradually increases with increasing β. The boundary layer thickness is reduced by increasing the effect of Maxwell parameter β.

In Figures 5(a)–5(c), the velocity, temperature, and concentration profiles are drafted against various values of unsteadiness parameter $M = 0 \cdot 1, 0 \cdot 5, 1 \cdot 0$,and $1 \cdot 5$ with some fixed parameters $\beta = 0 \cdot 3, S_c = 0 \cdot 7, \varepsilon = 1 \cdot 8, \gamma = 0 \cdot 4$, and $\Pr = 0 \cdot 3$. The most favorable change in each profile is noted against the unsteadiness parameter M in the presence of viscosity and chemical reaction effects. The velocity, temperature, and concentration increase at a minimum value of $M = 0 \cdot 1$ but decrease gradually with increasing M with prominent variations in the presence of ε. The increasing effect of unsteadiness parameter M exhibits the reduction in thickness of thermal boundary layer near the wall of stretching surface. In Figures 6(a)–6(c), the effects of viscosity parameter ε on skin friction $f''(\eta)$, heat transfer $-\theta'(\eta)$, and mass transfer $-\phi'(\eta)$ are clearly shown. The maximum value of $f''(\eta)$ and $-\phi'(\eta)$ is noted at a lower value of viscosity parameter ε, and this gradually decreases with increasing ε in the presence of chemical reaction. The decreasing behavior in mass transfer $-\phi'(\eta)$ is drafted by increasing ε but increases as ε decreases significantly.

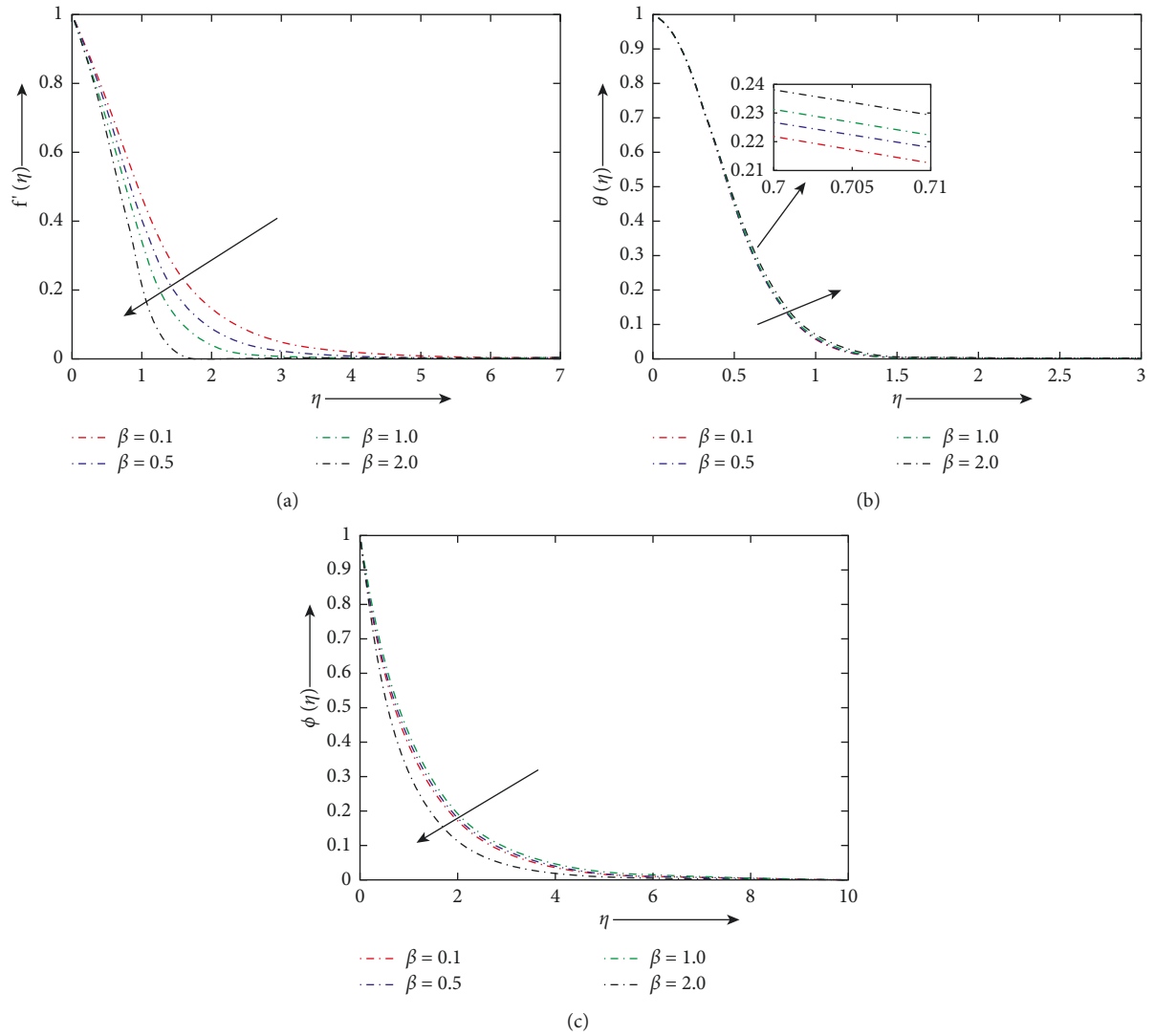

Figure 4: (a–c) Graphical representation of $\mathbf{f}'(\eta)$, $\theta(\eta)$, and $\phi(\eta)$ against Maxwell parameter β with some fixed parameters.

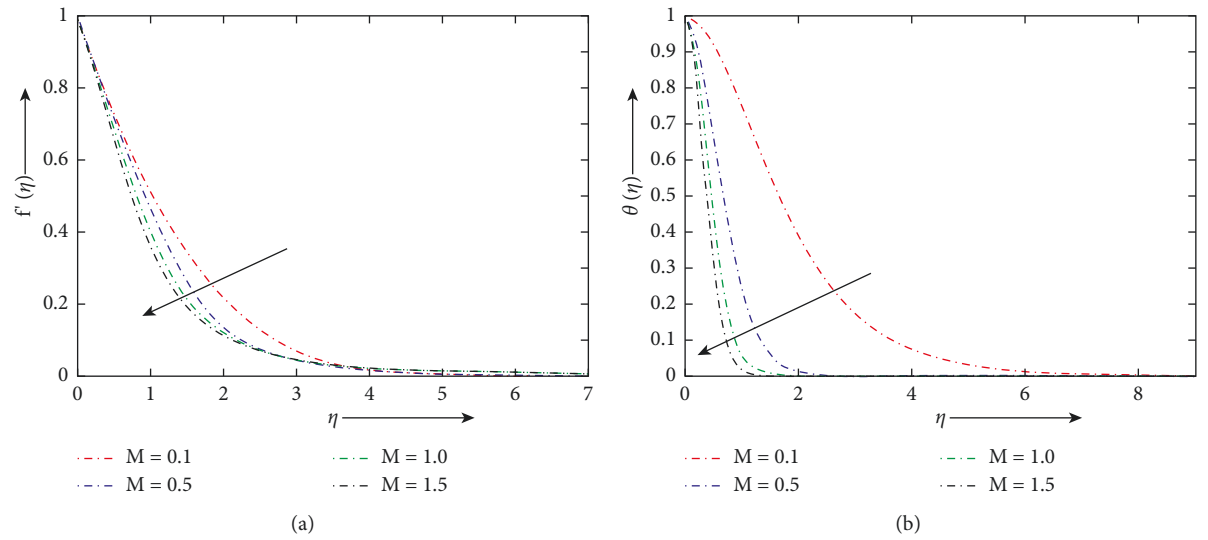

Figure 5: Continued.

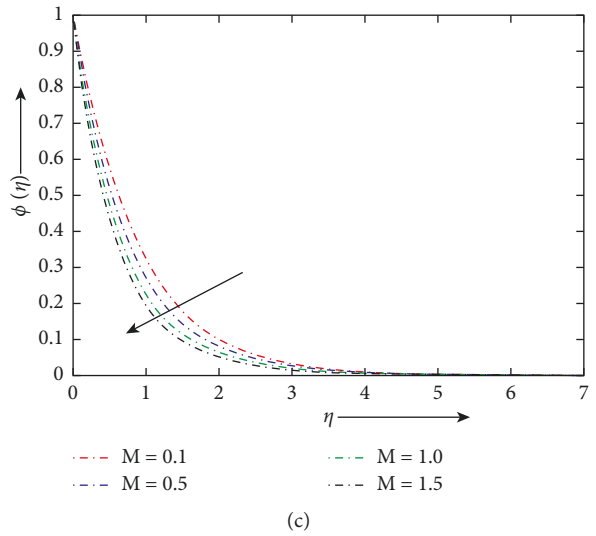

(c)

FIGURE 5: (a–c) Graphical representation of $\mathbf{f}'(\eta)$, $\theta(\eta)$, and $\phi(\eta)$ against unsteadiness parameter M with some fixe parameters.

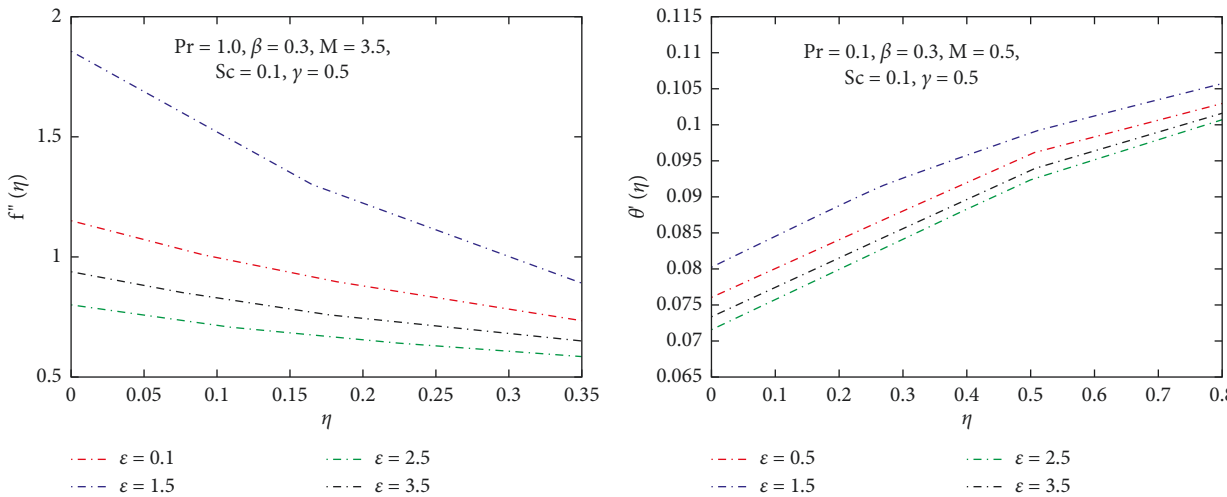

(a)

(b)

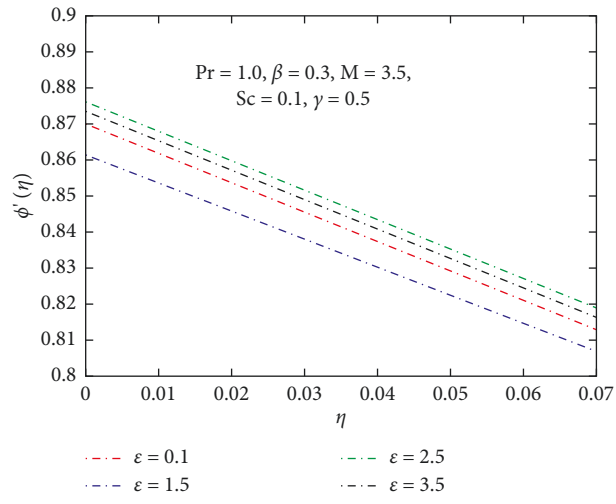

(c)

FIGURE 6: (a–c) Graphical representation of $\mathbf{f}''(\eta)$, $-\boldsymbol{\theta}'(\eta)$, and $-\boldsymbol{\phi}'(\eta)$ against temperature-dependent viscosity parameter ε with some fixed parameters.

4. Conclusion

The graphical and numerical outcomes of Maxwell fluid with variable viscosity and chemical reaction effects are executed for several values of dimensionless parameters involved in the equations such as the variable viscosity parameter (ε), the Prandtl number (Pr), the Maxwell parameter (β), and the unsteadiness parameter M. To illustrate the computed results, some figures are plotted and physical explanations are given for velocity $f'(\eta)$, concentration $\phi(\eta)$, and temperature $\theta(\eta)$ with their slopes skin friction $f''(\eta)$, mass transfer $-\phi\prime(\eta)$, and heat transfer $-\theta\prime(\eta)$, respectively. The main outcomes are given as follows:

(i) The fluid velocity is depicted maximum at a higher value of $\varepsilon = 1 \cdot 5$, while the minimum value of velocity profile is examined at a lower value of $\varepsilon = 0 \cdot 1$

(ii) The similar trend in concentration is examined for each value of Pr graphically but it increases with decreasing Pr by satisfying the given boundary conditions

(iii) The increasing effect of the unsteadiness parameter M exhibits the reduction in thickness of the thermal boundary layer near the wall of stretching surface

(iv) The maximum increasing behavior in temperature is depicted at a lower value of $\mathrm{Pr} = 0 \cdot 1$, but it decreases as the value of Pr increases with prominent variations.

(v) The maximum value of $f'\prime(\eta)$ and $-\theta'(\eta)$ is noted at a lower value of viscosity parameter ε, and it gradually decreases with increasing ε in the presence of chemical reaction.

Data Availability

No data were used to support this study.

Conflicts of Interest

The authors declare that they have no conflicts of interest.

References

[1] P. Siddheshwar, G. Sekhar, and A. Chethan, "Flow and heat transfer in a Newtonian liquid with temperature dependent properties over an exponential stretching sheet," *Journal of Applied Fluid Mechanics*, vol. 7, no. 2, pp. 367–374, 2014.

[2] S. Aman, Q. Al-Mdallal, and I. Khan, "Heat transfer and second order slip effect on mhd flow of fractional Maxwell fluid in a porous medium," *Journal of King Saud University Science*, vol. 32, no. 1, pp. 450–458, 2020.

[3] M. Abd El-Aziz, "Unsteady mixed convection heat transfer along a vertical stretching surface with variable viscosity and viscous dissipation," *Journal of the Egyptian Mathematical Society*, vol. 22, no. 3, pp. 529–537, 2014.

[4] M. S. Abel, S. K. Khan, and K. V. Prasad, "Study of viscoelastic fluid flow and heat transfer over a stretching sheet with variable viscosity," *International Journal of Non-linear Mechanics*, vol. 37, no. 1, pp. 81–88, 2002.

[5] I. A. Hassanien, "The effect of variable viscosity on flow and heat transfer on a continuous stretching surface," *ZAMM - Journal of Applied Mathematics and Mechanics/Zeitschrift für Angewandte Mathematik und Mechanik*, vol. 77, no. 11, pp. 876–880, 1997.

[6] M. Khan, M. Y. Malik, T. Salahuddin, S. Saleem, and A. Hussain, "Change in viscosity of Maxwell fluid flow due to thermal and solutal stratifications," *Journal of Molecular Liquids*, vol. 288, Article ID 110970, 2019.

[7] Y. Khan, Q. Wu, N. Faraz, and A. Yildirim, "The effects of variable viscosity and thermal conductivity on a thin film flow over a shrinking/stretching sheet," *Computers & Mathematics with Applications*, vol. 61, no. 11, pp. 3391–3399, 2011.

[8] S. Mukhopadhyay and K. Bhattacharyya, "Unsteady flow of a Maxwell fluid over a stretching surface in presence of chemical reaction," *Journal of the Egyptian Mathematical Society*, vol. 20, no. 3, pp. 229–234, 2012.

[9] K. R. Rajagopal, T. Y. Na, and A. S. Gupta, "Flow of a viscoelastic fluid over a stretching sheet," *Rheologica Acta*, vol. 23, no. 2, pp. 213–215, 1984.

[10] M. S. Abel, E. Sanjayanand, and M. M. Nandeppanavar, "Viscoelastic Mhd Flow and Heat Transfer over a Stretching Sheet with Viscous and Ohmic Dissipations," *Communications in Nonlinear Science and Numerical Simulation*, vol. 13, no. 9, pp. 1808–1821, 2008.

[11] R. Cortell, "Toward an understanding of the motion and mass transfer with chemically reactive species for two classes of viscoelastic fluid over a porous stretching sheet," *Chemical Engineering and Processing - Process Intensification*, vol. 46, no. 10, pp. 982–989, 2007.

[12] H. I. Andersson, O. R. Hansen, and B. Holmedal, "Diffusion of a chemically reactive species from a stretching sheet," *International Journal of Heat and Mass Transfer*, vol. 37, no. 4, pp. 659–664, 1994.

[13] B. S. Dandapat, B. Santra, and H. I. Andersson, "Thermocapillarity in a liquid film on an unsteady stretching surface," *International Journal of Heat and Mass Transfer*, vol. 46, no. 16, pp. 3009–3015, 2003.

[14] B. Dandapat, B. Santra, and K. Vajravelu, "The effects of variable fluid properties and thermo capillarity on the flow of a thin film on an unsteady stretching sheet," *International Journal of Heat and Mass Transfer*, vol. 50, no. 5-6, pp. 991–996, 2007.

[15] E. M. A. Elbashbeshy and M. A. A. Bazid, "Heat transfer over an unsteady stretching surface," *Heat and Mass Transfer*, vol. 41, no. 1, pp. 1–4, 2004.

[16] R. Tsai, K. H. Huang, and J. S. Huang, "Flow and heat transfer over an unsteady stretching surface with non-uniform heat source," *International Communications in Heat and Mass Transfer*, vol. 35, no. 10, pp. 1340–1343, 2008.

[17] T. Hayat and Z. Abbas, "Channel flow of a Maxwell fluid with chemical reaction," *Zeitschrift für Angewandte Mathematik und Physik*, vol. 59, no. 1, pp. 124–144, 2008.

[18] A. J. Chamkha, A. M. Aly, and M. A. Mansour, "Similarity solution for unsteady heat and mass transfer from a stretching surface embedded in a porous medium with suction/injection and chemical reaction effects," *Chemical Engineering Communications*, vol. 197, no. 6, pp. 846–858, 2010.

[19] K. Bhattacharyya, S. Mukhopadhyay, and G. C. Layek, "Slip effects on an unsteady boundary layer stagnation-point flow and heat transfer towards a stretching sheet," *Chinese Physics Letters*, vol. 28, no. 9, Article ID 094702, 2011.

[20] K. Bhattacharyya, "Effects of radiation and heat source/sink on unsteady mhd boundary layer flow and heat transfer over a

shrinking sheet with suction/injection," *Frontiers of Chemical Science and Engineering*, vol. 5, no. 3, pp. 376–384, 2011.

[21] P. S. Gupta and A. S. Gupta, "Heat and mass transfer on a stretching sheet with suction or blowing," *Canadian Journal of Chemical Engineering*, vol. 55, no. 6, pp. 744–746, 1977.

[22] A. Ishak, R. Nazar, and I. Pop, "Heat transfer over an unsteady stretching permeable surface with prescribed wall temperature," *Nonlinear Analysis: Real World Applications*, vol. 10, no. 5, pp. 2909–2913, 2009.

[23] S. Mukhopadhyay and K. Vajravelu, "Effects of Transpiration and Internal Heat Generation/absorption on the Unsteady Flow of a Maxwell Fluid at a Stretching Surface," *Applied Mechanics*, vol. 79, no. 4, Article ID 044508, 2012.